Journal of Physics: Conference Series **402** (2012) 012038 doi:10.1088/1742-6596/402/1/012038

Microscopic calculation of heavy-ion potentials based on TDHF

A S Umar and V E Oberacker

Department of Physics and Astronomy, Vanderbilt University, Nashville, TN 37235, USA

E-mail: umar@compsci.cas.vanderbilt.edu

Abstract. We present the numerical details of a new method for calculating ion-ion interaction potentials from time-dependent Hartree-Fock calculations using density as a constraint.

1. Introduction

The investigation of internuclear potentials for heavy-ion collisions is of fundamental importance for the study of fusion reactions as well as for the formation of superheavy elements and nuclei far from stability. Recently, we have developed a new method to extract ion-ion interaction potentials directly from the time-dependent Hartree-Fock (TDHF) time-evolution of the nuclear system [1]. In the density-constrained TDHF (DC-TDHF) approach the TDHF time-evolution takes place with no restrictions. At certain times during the evolution the instantaneous density is used to perform a static Hartree-Fock minimization while holding the neutron and proton densities constrained to be the corresponding instantaneous TDHF densities. In essence, this provides us with the TDHF dynamical path in relation to the multi-dimensional static energy surface of the combined nuclear system. In this approach there is no need to introduce constraining operators which assume that the collective motion is confined to the constrained phase space. In short, we have a self-organizing system which selects its evolutionary path by itself following the microscopic dynamics. Some of the effects naturally included in the DC-TDHF calculations are: neck formation, mass exchange, internal excitations, deformation effects to all order, as well as the effect of nuclear alignment for deformed systems. The DC-TDHF theory provides a comprehensive approach to calculating fusion barriers in the mean-field limit. The theory has been applied to calculate fusion cross-sections for ^{64}Ni+^{132}Sn, ^{64}Ni+^{64}Ni, ^{16}O+^{208}Pb, ^{70}Zn + ^{208}Pb, ^{48}Ca + ^{238}U, and ^{132,124}Sn+^{96}Zr systems [2, 3, 4, 5, 6, 7, 8]. In this paper we will outline the DC-TDHF method and give examples of its application to the calculation of fusion cross-sections for various systems.

2. Theory

In many branches of science, highly complex many-body systems are often described in macroscopic terms, this is particularly true in the case of relativistic and non-relativistic heavy-ion collisions. For example, the time evolution of the nuclear surface and the corresponding geometrical shape provides a very useful parameter to help organize experimental data. Using this approach numerous evolutionary models have been developed to explain particular aspects of experimental data. These methods provide a useful and productive means for quantifying

multitudinous reaction data. In practice, they require a quantitative understanding of the data as well as a clear physical picture of the important aspects of the reaction dynamics. The depiction of the collision must be given at the onset, including the choice of coordinates which govern the evolution of the reaction. Guessing the correct degrees of freedom is extremely hard, without a full understanding of the dynamics, and can easily lead to misbegotten results. More importantly, it is most often not possible to connect these macroscopic classical parameters, describing nuclear matter under extreme excitation and rearrangement, with the more fundamental properties of the nuclear force. Such difficulties can only be overcome with a fully microscopic theory of the collision dynamics.

2.1. Time-dependent Hartree-Fock method

The theoretical formalism for the microscopic description of complex many-body quantum systems and the understanding of the nuclear interactions that result in self-bound, composite nuclei possessing the observed properties are the underlying challenges for studying low energy nuclear physics. The Hartree-Fock approximation and its time-dependent generalization the time-dependent Hartree-Fock theory has provided a possible means to study the diverse phenomena observed in low energy nuclear physics [9].

Given a many-body Hamiltonian containing two and three-body interactions

$$H = \sum_{i}^{N} t_i + \sum_{i<j}^{N} v_{ij} + \sum_{i<j<k}^{N} v_{ijk} \ , \tag{1}$$

the time-dependent action S can be constructed as

$$S = \int_{t_1}^{t_2} dt < \Phi(t)|H - i\hbar\partial_t|\Phi(t) > \ . \tag{2}$$

Here, Φ denotes the time-dependent, many-body wavefunction, $\Phi(\mathbf{r_1}, \mathbf{r_2}, \ldots, \mathbf{r_A}; t)$, and t_i is the one-body kinetic energy operator. General variation of S recovers the time-dependent Schrödinger equation. In TDHF approximation the many-body wavefunction is replaced by a single Slater determinant and this form is preserved at all times. The determinental form guarantees the antisymmetry required by the Pauli principle for a system of fermions. In this limit, the variation of the action yields the most probable time-dependent path between points t_1 and t_2 in the multi-dimensional space-time phase space

$$\delta S = 0 \rightarrow \Phi(t) = \Phi_0(t) \ . \tag{3}$$

In practice $\Phi_0(t)$ is chosen to be a Slater determinant

$$\Phi_0(t) = \frac{1}{\sqrt{N!}} det|\phi_\lambda(\mathbf{r}\,, t)| \ , \tag{4}$$

where $\phi_\lambda(\mathbf{r}\,, t)$ are the single-particle states with quantum numbers λ. If the variation in Eq.(3) is performed with respect to the single-particle states ϕ^*_λ we obtain a set of coupled, nonlinear, self-consistent initial value equations for the single-particle states

$$h\left(\{\phi_\mu\}\right)\phi_\lambda = i\hbar\dot{\phi_\lambda} \qquad \lambda = 1, ..., N \ . \tag{5}$$

These are the fully microscopic time-dependent Hartree-Fock equations which preserve the major conservation laws such as the particle number, total energy, total angular momentum, etc. As we see from Eq.(5), each single-particle state evolves in the mean-field generated by the concerted

action of all the other single-particle states. Static equations can be obtained from Eq.(5) by taking out a trivial phase from the single-particle states

$$\begin{aligned} h(\{\chi_\mu\})\chi_\lambda &= \epsilon_\lambda \chi_\lambda \\ \phi_\lambda(\mathbf{r}\,,t) &= e^{-i\epsilon_\lambda t/\hbar}\chi_\lambda(\mathbf{r}\,)\,. \end{aligned} \tag{6}$$

In TDHF, the initial nuclei are calculated using the static Hartree-Fock (HF) theory. The resulting Slater determinants for each nucleus comprise the larger Slater determinant describing the colliding system during the TDHF evolution. Nuclei are assumed to move on a pure Coulomb trajectory until the initial separation between the nuclear centers used in TDHF evolution. Using the Coulomb trajectory we compute the relative kinetic energy at this separation and the associated translational momenta for each nucleus. The nuclei are than boosted by multiplying the HF states with

$$\Phi_j \rightarrow \exp(\imath \mathbf{k}_j \cdot \mathbf{R})\Phi_j\,, \tag{7}$$

where Φ_j is the HF state for nucleus j and $\mathbf{R}$ is the corresponding center of mass coordinate

$$\mathbf{R} = \frac{1}{A_j}\sum_{i=1}^{A_j}\mathbf{r}_i\,. \tag{8}$$

The Galilean invariance of the TDHF equations assures the evolution of the system without spreading and the conservation of the total energy for the system. In TDHF, the many-body state remains a Slater determinant at all times. The final state is a filled determinant, even in the case of two well separated fragments. This phenomenon is commonly known as the "cross-channel coupling" and indicates that it is not possible to identify the well separated fragments as distinct nuclei since each single particle state will have components distributed everywhere in the numerical box. In this sense it is only possible to extract *inclusive* (averaged over all states) information from these calculations.

2.2. DC-TDHF method

The concept of using density as a constraint for calculating collective states from TDHF time-evolution was first introduced in Ref. [10], and used in calculating collective energy surfaces in connection with nuclear molecular resonances in Ref. [11].

In this approach we assume that a collective state is characterized only by density ρ, and current $\mathbf{j}$. This state can be constructed by solving the static Hartree-Fock equations

$$< \Phi_{\rho,\mathbf{j}}|a_h^\dagger a_p \hat{H}|\Phi_{\rho,\mathbf{j}} >= 0\,, \tag{9}$$

subject to constraints on density and current

$$\begin{aligned} < \Phi_{\rho,\mathbf{j}}|\hat{\rho}(\mathbf{r})|\Phi_{\rho,\mathbf{j}} > &= \rho(\mathbf{r},t) \\ < \Phi_{\rho,\mathbf{j}}|\hat{j}(\mathbf{r})|\Phi_{\rho,\mathbf{j}} > &= \mathbf{j}(\mathbf{r},t)\,. \end{aligned}$$

Choosing $\rho(\mathbf{r},t)$ and $\mathbf{j}(\mathbf{r},t)$ to be the instantaneous TDHF density and current results in the lowest energy collective state corresponding to the instantaneous TDHF state $|\Phi(t)>$, with the corresponding energy

$$E_{coll}(\rho(t),\mathbf{j}(t)) =< \Phi_{\rho,\mathbf{j}}|\hat{H}|\Phi_{\rho,\mathbf{j}} > \ . \tag{10}$$

This collective energy differs from the conserved TDHF energy only by the amount of internal excitation present in the TDHF state, namely

$$E^*(t) = E_{TDHF} - E_{coll}(t)\,. \tag{11}$$

However, in practical calculations the constraint on the current is difficult to implement but we can define instead a static adiabatic collective state $|\Phi_\rho>$ subject to the constraints

$$\begin{aligned} <\Phi_\rho|\hat{\rho}(\mathbf{r})|\Phi_\rho> &= \rho(\mathbf{r},t) \\ <\Phi_\rho|\hat{j}(\mathbf{r})|\Phi_\rho> &= 0\ . \end{aligned}$$

In terms of this state one can write the collective energy as

$$E_{coll} = E_{kin}(\rho(t),\mathbf{j}(t)) + E_{DC}(\rho(\mathbf{r},t))\ , \tag{12}$$

where the density-constrained energy E_{DC}, and the collective kinetic energy E_{kin} are defined as

$$\begin{aligned} E_{DC} &= <\Phi_\rho|\hat{H}|\Phi_\rho> \\ E_{kin} &\approx \frac{m}{2}\sum_q \int d^3r\ \mathbf{j}_q^2(t)/\rho_q(t)\ , \end{aligned}$$

where the index q is the isospin index for neutrons and protons ($q = n, p$). From Eq. 12 is is clear that the density-constrained energy E_{DC} plays the role of a collective potential. In fact this is exactly the case except for the fact that it contains the binding energies of the two colliding nuclei. One can thus define the ion-ion potential as [1]

$$V = E_{\rm DC}(\rho(\mathbf{r},t)) - E_{A_1} - E_{A_2}\ , \tag{13}$$

where E_{A_1} and E_{A_2} are the binding energies of two nuclei obtained from a static Hartree-Fock calculation with the same effective interaction. For describing a collision of two nuclei one can label the above potential with ion-ion separation distance $R(t)$ obtained during the TDHF time-evolution. This ion-ion potential $V(R)$ is asymptotically correct since at large initial separations it exactly reproduces $V_{Coulomb}(R_{max})$. In addition to the ion-ion potential it is also possible to obtain coordinate dependent mass parameters. One can compute the "effective mass" $M(R)$ using the conservation of energy

$$M(R) = \frac{2[E_{\rm c.m.} - V(R)]}{\dot{R}^2}\ , \tag{14}$$

where the collective velocity $\dot{R}$ is directly obtained from the TDHF evolution and the potential $V(R)$ from the density constraint calculations.

2.3. Skyrme interaction

Almost all TDHF calculations have been done using the Skyrme interaction. A variety of calculations have shown that the TDHF results are very sensitive to the different parametrization of the Skyrme force [12]. The Skyrme energy density functional contains terms which depend on the nuclear density, ρ, kinetic-energy density, τ, spin density, $\mathbf{s}$, spin kinetic energy density, $\mathbf{T}$, and the full spin-current pseudotensor, $\mathbf{J}$, as

$$E = \int d^3r\ \mathcal{H}(\rho,\tau,\mathbf{j},\mathbf{s},\mathbf{T},\mathbf{J};\mathbf{r})\ . \tag{15}$$

The time-odd terms ($\mathbf{j}$, $\mathbf{s}$, $\mathbf{T}$) vanish for static calculations of even-even nuclei, while they are present for odd mass nuclei, in cranking calculations, as well as in TDHF. The spin-current pseudotensor, $\mathbf{J}$, is time-even and does not vanish for static calculations of even-even nuclei. Our TDHF program includes all of the time-odd terms in the Skyrme interaction.

3. Numerical methods

In this section we discuss the numerical details of performing TDHF calculations of nuclear collisions as well as the density-constraint method, which is crucial for ion-ion potential calculations.

3.1. Discrete variation and lattice equations

The lattice solution of differential equations on a discretized mesh of independent variables may be viewed to proceed in two steps: (1) Obtain a discrete representation of the functions and operators on the lattice. (2) Solve the resulting lattice equations using iterative techniques. Step (1) is an interpolation problem for which we could take advantage of the techniques developed using the basis-spline functions [13]. The use of the basis-spline collocation method leads to a matrix-vector representation on the collocation lattice with a metric describing the transformation properties of the collocation lattice.

In order to obtain a set of lattice equations which preserve the conservation laws associated with the continuous equations it is essential to develop a modified variational approach. This goal is achieved by performing a variation to the discretized form of a conserved quantity, i.e. total energy. Consequently, the resulting equations will preserve all of the conserved quantities on the lattice. For the TDHF equations we consider a general discretized form of the action

$$S = \int dt \sum_{\alpha\beta\gamma} \Delta V_{\alpha\beta\gamma} \left\{ \mathcal{H}(\alpha\beta\gamma) - \left[i\hbar \sum_{\mu} \psi^*_{\mu}(\alpha\beta\gamma) \frac{\partial \psi_{\mu}}{\partial t}(\alpha\beta\gamma) \right] \right\} , \tag{16}$$

where indices α, β, γ denote the lattice points in three-dimensional space, and $\Delta V_{\alpha\beta\gamma}$ is the corresponding infinitesimal volume element. Due to the presence of derivative operators in the Hamiltonian the explicit form of these expressions will depend non-locally on the lattice indices. The general variation, which preserves the properties of the continuous variation, is given by

$$\frac{\delta \psi^*_{\mu}(\alpha\beta\gamma)}{\delta \psi^*_{\lambda}(\alpha'\beta'\gamma')} = \frac{1}{\Delta V_{\alpha\beta\gamma}} \delta_{\lambda\mu} \delta_{\alpha'\alpha} \delta_{\beta'\beta} \delta_{\gamma'\gamma} \, . \tag{17}$$

Until recently, most HF and TDHF calculations have been performed using finite-difference lattice techniques. The details of the discrete variation for the finite-difference case are given in Refs. [14, 15]. Below we outline a procedure for using the BSCM for the numerical solution of HF and TDHF equations. Further details of the BSCM is published elsewhere [13].

3.2. Basis-splines

Given a set of points or *knots* denoted by the set $\{x_i\}$ a basis-spline (B-spline denoted by B_i^M) function of order M is constructed from continuous piecewise polynomials of order $M-1$ [16]. B-splines have continuous derivatives up to $(M-2)^{nd}$ derivative and a discontinuous $(M-1)^{st}$ derivative. We only consider odd order splines or even order polynomials for reasons related to the choice of the collocation points. The i^{th} B-spline is nonzero only in the interval (x_i, x_{i+M}). This property is commonly referred to as limited support. The knots are the points where polynomials that make up the B-spline join. In the interval containing the tail region B-splines fall off very rapidly to zero. An example of order $M = 5$ splines extending over a physical region is illustrated in Fig.1. We can also construct exact derivatives of B-splines provided the derivative order does not exceed $M-1$.

A continuous function $f(x)$, defined in the interval (x_{min}, x_{max}), can be expanded in terms of B-spline functions as

$$f(x) = \sum_i B_i^M(x) c^i \, , \tag{18}$$

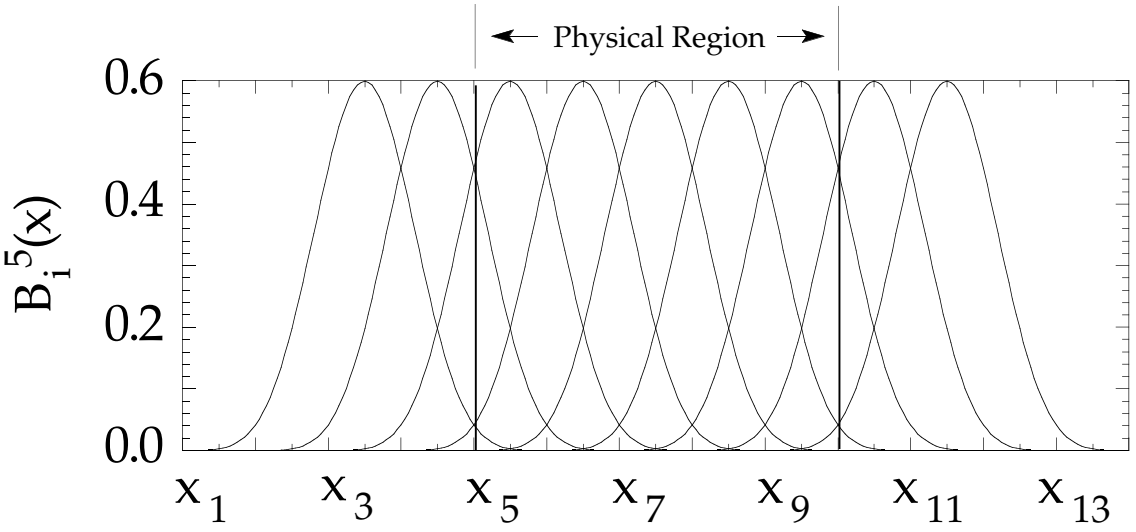

Figure 1. A region of space with physical boundaries located at knots x_M and x_{M+N} for $M = 5$ and $N = 5$. The B-spline B_1^M which begins at the first knot x_1 has its tail in the physical region. The last B-spline which begins within the physical boundaries is B_{N+M-1}^M. It extends up to the last knot x_{N+2M-1}.

where quantities c^i denote the expansion coefficients. We can solve for the expansion coefficients in terms of a given (or to be determined) set of function values evaluated at a set of data points more commonly known as *collocation points*. There are a number of ways to choose collocation points [16, 13], however, for odd order B-splines a simple choice is to place one collocation point at the center of each knot interval within the physical boundaries

$$x_\alpha = \frac{x_{\alpha+M-1} + x_{\alpha+M}}{2} \quad , \quad \alpha = 1, \ldots, N. \tag{19}$$

Here, $x_M = x_{min}$, $x_{N+M} = x_{max}$, and N is the number of collocation points. We can now write a linear system of equations by evaluating (18) at these collocation points

$$f_\alpha = \sum_i B_{\alpha i} c^i \ , \tag{20}$$

where $f_\alpha \equiv f(x_\alpha)$, and $B_{\alpha i} \equiv B_i^M(x_\alpha)$. In order to solve for the expansion coefficients the matrix $\mathbf{B}$ needs to be inverted. However, as it stands matrix $\mathbf{B}$ is not a square matrix, since the total number of B-splines with a nonzero extension in the physical region is $N + M - 1$. In order to perform the inversion we need to introduce additional linear equations which represent the boundary conditions imposed on $f(x)$ at the two boundary points, x_M and x_{M+N}. The essence of the lattice method is to eliminate the expansion coefficients c^i using this inverse matrix. The details of using the boundary conditions (or periodic boundaries) and inverting the resulting square matrix are discussed in Ref. [13]. Following the inversion the coefficients are given by

$$c^i = \sum_\alpha \left[\mathbf{B}^{-1}\right]^{i\alpha} f_\alpha \ . \tag{21}$$

One can trivially show that all local functions will have a local representation in the finite dimensional collocation space

$$f(x) \longrightarrow f_\alpha \ . \tag{22}$$

The collocation representation of the operators can be obtained by considering the action of an operator $\mathcal{O}$ onto a function $f(x)$

$$\mathcal{O}f(x) = \sum_i [\mathcal{O}B_i^M(x)]c^i \ . \tag{23}$$

If we evaluate the above expression at the collocation points x_α we can write

$$[\mathcal{O}f]_\alpha = \sum_i [\mathcal{O}B]_{\alpha i} c^i \ . \tag{24}$$

Substituting from Eq. (21) for the coefficients c^i we obtain

$$\begin{aligned} [\mathcal{O}f]_\alpha &= \sum_{i\beta} [\mathcal{O}B]_{\alpha i} \left[\mathbf{B}^{-1}\right]^{i\beta} f_\beta \\ &= \sum_\beta O_\alpha^\beta f_\beta \ , \end{aligned} \tag{25}$$

where we have defined the collocation space matrix representation of the operator $\mathcal{O}$ by

$$O_\alpha^\beta = \sum_i [\mathcal{O}B]_{\alpha i} \left[\mathbf{B}^{-1}\right]^{i\beta} \ . \tag{26}$$

Notice that the construction of the collocation space operators can be performed once and for all at the beginning of a calculation, using only the given knot sequence and collocation points. Due to the presence of the inverse in Eq. (26) the matrix O is not sparse. In practice, operator $\mathcal{O}$ is chosen to be a differential operator such as d/dx or d^2/dx^2. By a similar construction it is also possible to obtain the appropriate integration weights on the collocation lattice [13].

3.3. Discrete HF equations

Since the detailed derivation of the BSCM representation of the TDHF equations involve many terms that are present in the energy functional, we will only show few terms. The three-dimensional expansion in terms of B-splines is a simple generalization of Eq. (18)

$$\psi_\lambda(x,y,z) = \sum_{ijk} c_\lambda^{ijk} B_i(x) B_j(y) B_k(z) \ . \tag{27}$$

The knots and collocation points for each coordinate can be different. With the appropriate definition of boundary conditions all of the discretization techniques discussed in the previous section can be generalized to the three-dimensional space. The details of this procedure are given in [13].

As an example for a local term let us consider a part of the t_0 contribution to the total energy

$$\frac{t_0}{2}(1+\frac{x_0}{2}) \int d^3r \rho^2 = \frac{t_0}{2}(1+\frac{x_0}{2}) \sum_{\alpha\beta\gamma} w^\alpha w^\beta w^\gamma [\rho(\alpha\beta\gamma)]^2 \ , \tag{28}$$

where on the right-hand side we have written the discretized form on a collocation lattice with collocation weights denoted by w. Here, α, β, γ represent the collocation points in x, y, and z directions, respectively. In order to be able to perform the variation with respect to the single-particle states ψ_λ^* we rewrite equation (28) explicitly

$$\frac{t_0}{2}(1+\frac{x_0}{2}) \sum_{\alpha\beta\gamma} w^\alpha w^\beta w^\gamma \sum_{\mu\nu} \psi_\mu^* \psi_\mu \psi_\nu^* \psi_\nu \ . \tag{29}$$

Using Eq.(17) in the variation of Eq.(29) we obtain (after replacing the primed indices with unprimed ones) the contribution

$$t_0(1+\frac{x_0}{2})\rho(\alpha\beta\gamma)\psi_\lambda(\alpha\beta\gamma)\ , \tag{30}$$

where we have rewritten a summation as the total density. The same procedure can be carried out for the nonlocal terms in the energy density. A typical term is illustrated below

$$\begin{aligned}(\boldsymbol{\nabla}\psi^{\pm}_{\lambda})_{\alpha\beta\gamma} &= \sum_{\alpha'} D^{\alpha'}_{\alpha}\psi^{\pm}_{\lambda}(\alpha'\beta\gamma)\,\hat{\imath} + \sum_{\beta'} D^{\beta'}_{\beta}\psi^{\pm}_{\lambda}(\alpha\beta'\gamma)\,\hat{\jmath} \\ &+ \sum_{\gamma'} D^{\gamma'}_{\gamma}\psi^{\pm}_{\lambda}(\alpha\beta\gamma')\,\hat{k}\end{aligned}$$

where the matrices $\mathbf{D}$ denote the first derivative matrices in x, y, z directions (they can be different although the notation does not make this obvious), calculated as described in the previous section. Finally, the HF equations can be written as matrix-vector equations on the collocation lattice

$$h\psi^{\pm}_{\lambda} \longrightarrow \mathbf{h}\cdot\boldsymbol{\psi}^{\pm}_{\lambda}\ . \tag{31}$$

The essence of this construction is that the terms in the single-particle Hamiltonian $\mathbf{h}$ are matrices in one coordinate and diagonal in others. Therefore, $\mathbf{h}$ need not be stored as a full matrix, which allows the handling of very large systems directly in memory. The details of this procedure are discussed below.

3.4. Solution of the discrete equations

In this subsection we will outline some of the numerical methods developed for the solution of the discretized HF and TDHF equations. The subsection is divided into two parts; first part discusses the static iteration methods and the solution of the field equations and in particular the powerful damped relaxation method [17]. In addition we discuss the implementation of external constraints on the HF equations. The second part of the subsection introduces a number of time-evolution methods used in our calculations. Typical numerical accuracies are also discussed.

3.4.1. Static solutions The solution of the HF equations (31) represent the problem of finding the few lowest eigenvalues of a very large Hamiltonian matrix. Furthermore, due to the fact that we are dealing with a self-consistent problem the matrix elements must be recalculated at every iteration. However, in practice the matrix elements need not be stored. Instead, one can make use of the inherent sparsity to dynamically construct the operation of the single-particle Hamiltonian onto a statevector. The basic operation is

$$\boldsymbol{\psi}' = \mathbf{h}\cdot\boldsymbol{\psi}\ , \tag{32}$$

where the construction of the right hand side is done by explicitly programming the required linear combinations of the elements of $\boldsymbol{\psi}$ to give $\boldsymbol{\psi}'$. In this approach the only storage requirements are for the statevectors and small matrices present in the Hamiltonian.

The lattice equations are solved by using the damped relaxation method described in Refs. [11, 17]. A simple way for introducing the damped relaxation method is by pointing out its resemblance to the so-called imaginary time method. A more formal discussion is given in Ref. [17] where the generalization to the relativistic Dirac equation is also introduced. We start with the TDHF equations

$$i\hbar\frac{\partial\boldsymbol{\psi}_\lambda}{\partial t} = \mathbf{h}(t)\boldsymbol{\psi}_\lambda\ . \tag{33}$$

In terms of the discretized time $t_n = n\Delta t$ the solution at time $n+1$ can be obtained from time n by (see below)

$$\boldsymbol{\psi}_\lambda^{n+1} = e^{-i\Delta t \mathbf{h}^n/\hbar}\boldsymbol{\psi}_\lambda^n \,, \tag{34}$$

where $\mathbf{h}^n$ is the single-particle Hamiltonian at the n^{th} iteration. The imaginary time-step method consists of the transformation $\Delta t \to -i\Delta t$

$$\boldsymbol{\chi}_\lambda^{n+1} = e^{-x_0(\mathbf{h}^n - \epsilon_\lambda^n)}\boldsymbol{\chi}_\lambda^n \,, \tag{35}$$

where $x_0 = \Delta t/\hbar$, and we have taken out a trivial phase from $\boldsymbol{\psi}_\lambda^n$. The expansion of the exponential to first order in x_0 yields the imaginary time iteration scheme

$$\boldsymbol{\chi}_\lambda^{n+1} = \mathcal{O}[\boldsymbol{\chi}_\lambda^n - x_0(\mathbf{h}^n - \epsilon_\lambda^n)\boldsymbol{\chi}_\lambda^n] \,. \tag{36}$$

where $\mathcal{O}$ stands for Gram-Schmidt orthonormalization, which is necessary to ensure the orthonormality of the single-particle states at each iteration. In Eq. (36) the index n is no longer associated with time and it simply becomes an iteration counter. It is clear from Eq. (35) that the exponential acts as a filter in selecting the lowest eigenvalues of $\mathbf{h}$ and leads to the minimization of the HF energy. The generalization of the imaginary time method, where we introduce the damping matrix $\mathbf{D}$, results in the damped relaxation method

$$\boldsymbol{\chi}_\lambda^{n+1} = \mathcal{O}[\boldsymbol{\chi}_\lambda^n - x_0\mathbf{D}(E_0)(\mathbf{h}^n - \epsilon_\lambda^n)\boldsymbol{\chi}_\lambda^n] \,. \tag{37}$$

The damping operator $\mathbf{D}$ is chosen to be

$$\begin{aligned} \mathbf{D}(E_0) &= \left[1 + \frac{\mathbf{T}}{E_0}\right]^{-1} \\ &\approx \left[1 + \frac{\mathbf{T}_x}{E_0}\right]^{-1}\left[1 + \frac{\mathbf{T}_y}{E_0}\right]^{-1}\left[1 + \frac{\mathbf{T}_z}{E_0}\right]^{-1} \,, \end{aligned}$$

where $\mathbf{T}$ denotes the kinetic energy operator. Limits can be established for the ranges of the parameters x_0 and E_0 [17], but in practice fine-tuning is necessary for optimal performance. Two convergence criteria are used in practical calculations; one being the fractional change in the HF energy

$$\Delta E^n = \frac{E^{n+1} - E^n}{E^n} \,, \tag{38}$$

and other the fluctuations in energy

$$\eta \equiv \sqrt{< H^2 > - < H >^2} \,. \tag{39}$$

The fluctuations are a more stringent condition than the simple energy difference between two iterations. In practice, we have required η to be less than 10^{-6}. For this value of the energy fluctuation the fractional change in the HF energy is about 10^{-13}.

The calculation of the HF Hamiltonian also requires the evaluation of the direct Coulomb contribution. However, since the calculation of the three-dimensional Coulomb integral is very costly, instead one could solve the corresponding differential equation

$$\nabla^2 U_C(\mathbf{r}\,) = -4\pi e^2 \rho_p(\mathbf{r}\,) \,. \tag{40}$$

Details of solving the Poisson equation using the BSCM is given in Ref. [13].

3.4.2. Constrained HF calculations It is sometimes desirable to solve the static HF equations away from the global minimum in energy. Such situations usually arise in the study of fission barriers and in the study of long-lived superdeformed states of nuclei that can be formed during low energy heavy-ion collisions. These methods have been instrumental for the understanding of the formation of nuclear molecules [11]. All of these cases require the existence of a stable minimum which does not coincide with the ground state configuration. The usual approach is to study the HF energy of a nuclear system by keeping certain macroscopic degrees of freedom at pre-specified values. This results in a multi-dimensional *energy surface* from which extremum values can be obtained. The reliability of these results depend strongly on the correct identification of the relevant macroscopic degrees of freedom. However, as we will see below a special constrained HF method, *density constrained HF*, has also been developed which allows the minimization of the energy along a TDHF trajectory.

The goal is to devise an iteration scheme such that the expectation value of an arbitrary operator $\hat{Q}$ does not change from one static iteration to next

$$\sum_{\lambda} < \chi_{\lambda}^{n+1}|\hat{Q}|\chi_{\lambda}^{n+1} >= \sum_{\lambda} < \chi_{\lambda}^{n}|\hat{Q}|\chi_{\lambda}^{n} > \ . \tag{41}$$

Furthermore, we require this expectation value to be a fixed number Q_0. A procedure can be developed by using Lagrange multipliers that are dynamically adjusted [11]. We start with the static HF iteration scheme modified by the addition of a constraint (we have omitted the damping matrix $\mathbf{D}$ in the equations below for simplicity)

$$\boldsymbol{\chi}_{\lambda}^{n+1} = \mathcal{O}[\boldsymbol{\chi}_{\lambda}^{n} - x_0(\mathbf{h}^n + \lambda\hat{Q} - \epsilon_{\lambda}^{n})\boldsymbol{\chi}_{\lambda}^{n}] \ . \tag{42}$$

In Ref.[11] we give a set of exact equations which preserve the expectation of the constraining operator to order x_0^2. However, these equations involve the calculation of exchange terms and may become costly. Instead, one can develop a simpler iterative scheme as follows. Perform an intermediate step

$$\boldsymbol{\chi}_{\lambda}^{n+1/2} = \mathcal{O}[\boldsymbol{\chi}_{\lambda}^{n} - x_0(\mathbf{h}^n + \lambda^n\hat{Q} - \epsilon_{\lambda}^{n})\boldsymbol{\chi}_{\lambda}^{n}] \ , \tag{43}$$

and calculate the difference

$$\delta Q^{n+1/2} = \sum_{\lambda} < \chi_{\lambda}^{n+1/2}|\hat{Q}|\chi_{\lambda}^{n+1/2} > - \sum_{\lambda} < \chi_{\lambda}^{n}|\hat{Q}|\chi_{\lambda}^{n} > \ . \tag{44}$$

In analogy with the exact case the Lagrange parameter λ is altered to reduce this difference

$$\lambda^{n+1} = \lambda^n + c_0 \frac{\delta Q^{n+1/2}}{2x_0 \sum_{\lambda} < \chi_{\lambda}^{n}|\hat{Q}^2|\chi_{\lambda}^{n} > + d_0} \ , \tag{45}$$

where c_0 and d_0 are empirical parameters replacing the exchange terms. In terms of these intermediate states the $(n+1)st$ step is given by

$$\boldsymbol{\chi}_{\lambda}^{n+1} = \mathcal{O}[\boldsymbol{\chi}_{\lambda}^{n+1/2} - x_0(\lambda^{n+1} - \lambda^n + \delta\lambda^n)\hat{Q}\boldsymbol{\chi}_{\lambda}^{n+1/2}] \ , \tag{46}$$

where

$$\delta\lambda^n = \frac{\sum_{\lambda} < \chi_{\lambda}^{n}|\hat{Q}|\chi_{\lambda}^{n} > - Q_0}{2x_0 \sum_{\lambda} < \chi_{\lambda}^{n}|\hat{Q}^2|\chi_{\lambda}^{n} > + d_0} \ . \tag{47}$$

The extension of the method which allows the entire density to be constrained is straightforward. In this case we would like to constrain a continuous density

$$\rho^n(\mathbf{r}\,) = \sum_{\lambda} |\chi_{\lambda}^{n}(\mathbf{r}\,)|^2 \ , \tag{48}$$

to be equal to $\rho_0(\mathbf{r})$. The constraining operator $\hat{Q}$ becomes the density operator $\hat{\rho}(\mathbf{r})$ defined in the single-particle space

$$< \chi^n_\lambda | \hat{\rho}(\mathbf{r}) | \chi^n_\lambda >= |\chi^n_\lambda(\mathbf{r})|^2 \tag{49}$$

and the product $\lambda\hat{Q}$ is replaced by an integral

$$\lambda\hat{Q} \longrightarrow \int d^3r\, \lambda(\mathbf{r})\hat{\rho}(\mathbf{r}) = \lambda(\mathbf{r}) \; . \tag{50}$$

The last equality is due to the fact that in coordinate space $\hat{\rho}(\mathbf{r})$ is a delta function. An iterative scheme for $\lambda^n(\mathbf{r})$ is given by

$$\lambda^{n+1}(\mathbf{r}) = \lambda^n(\mathbf{r}) + c_0 \frac{\delta\rho^{n+1/2}}{2x_0\rho^n(\mathbf{r}) + d_0} \; , \tag{51}$$

where

$$\delta\rho^{n+1/2}(\mathbf{r}) \equiv \rho^{n+1/2}(\mathbf{r}) - \rho_0(\mathbf{r}) \tag{52}$$

is obtained from half-time iteration step

$$\boldsymbol{\chi}^{n+1/2}_\lambda = \mathcal{O}[\boldsymbol{\chi}^n_\lambda - x_0(\mathbf{h}^n + \lambda^n(\mathbf{r}) - \epsilon^n_\lambda)\boldsymbol{\chi}^n_\lambda] \; . \tag{53}$$

Note that in these equations we require that the density remain equal to $\rho_0(\mathbf{r})$ at every iteration and not just at the final step. Using these wavefunctions the full iteration can be written as

$$\boldsymbol{\chi}^{n+1}_\lambda = \mathcal{O}[\boldsymbol{\chi}^{n+1/2}_\lambda - x_0(\lambda^{n+1}(\mathbf{r}) - \lambda^n(\mathbf{r}) + \delta\lambda^n(\mathbf{r}))\boldsymbol{\chi}^{n+1/2}_\lambda] \; , \tag{54}$$

where

$$\delta\lambda^n(\mathbf{r}) = c_0 \frac{\rho^n(\mathbf{r}) - \rho_0(\mathbf{r})}{2x_0\rho_0(\mathbf{r}) + d_0} \; . \tag{55}$$

During the density constrained HF iterations the single-particle states readjust to minimize the energy while the initial density is kept fixed. In practical calculations the parameter x_0 has been replaced by the damping operator and the constants c_0 and d_0 were chosen to be 1.9 and 5×10^{-5}, respectively.

3.4.3. Time evolution The formal solution of the TDHF equations (5) is

$$\psi_\lambda(t) = U(t, t_0)\psi_\lambda(t_0) \; , \tag{56}$$

where we have omitted the spatial coordinates for simplicity and the time propagator $U(t, t_0)$ is given by

$$U(t, t_0) = \mathcal{T}\, exp\left[\frac{-i}{\hbar}\int_{t_0}^{t} dt' h(t')\right] \; . \tag{57}$$

The quantity $\mathcal{T}$ denotes time-ordering which is necessary in the general case. In practical calculations we discretize time as

$$t_n = n\Delta t \qquad\qquad n = 0, 1, 2, ...N \; , \tag{58}$$

and express the evolution operator in successive infinitesimal pieces

$$U(t, t_0) = U(t, t_{N-1})U(t_{N-1}, t_{N-2})...U(t_1, t_0) \; . \tag{59}$$

In this case the time-ordering operator can be ignored. For three-dimensional calculations the exponential operator is expanded as a Taylor series

$$U(t_{n+1}, t_n) \approx \left(1 + \sum_{k=1}^{K} \frac{(-i\Delta t\, \mathbf{h}/\hbar)^k}{k!}\right) . \tag{60}$$

The expansion of the operator requires repeated applications of $\mathbf{h}$ onto the wavefunctions. In practice, only $6-8$ terms are needed for the conservation of the norm at 1 part in 10^{-10} level during the entire time-evolution. The expansion method is also attractive due to the fact that it only involves matrix vector operations which could be easily customized for vector or parallel computers.

4. Applications

In this section we give examples of DC-TDHF calculation of potential barriers and fusion cross-sections. Calculations were done in 3-D geometry and using the full Skyrme force (SLy4) [12] without the center-of-mass correction as described in Ref. [18, 19]. We have performed density constraint calculations every 20 time steps. For the calculation of the ion-ion separation distance R we use the hybrid method, which relates the coordinate to the quadrupole moment for small R values, as described in Ref. [6]. The accuracy of the density constraint calculations is commensurate with the accuracy of the static calculations.

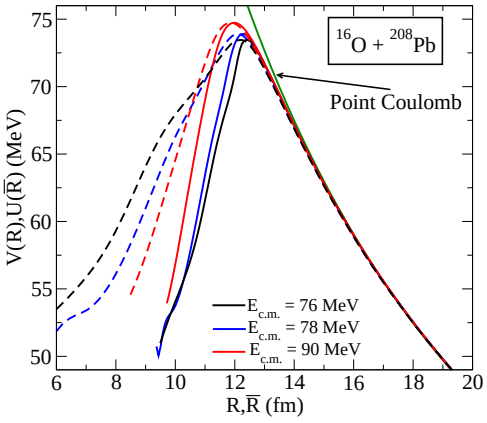

Figure 2. Potential barriers obtained from density constraint TDHF calculations at three different energies. The three dashed curves correspond to the transformed potential using coordinate dependent masses.

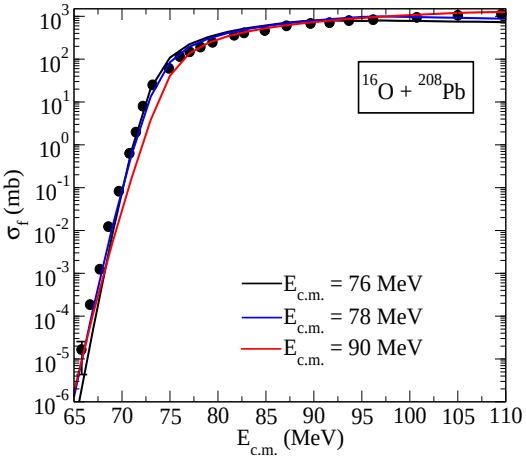

Figure 3. Total fusion cross section as a function of c.m. energy using the potentials of Fig. 2. The three curves correspond to the transformed potential using coordinate dependent masses.

4.1. Spherical system

The DC-TDHF method is expected to do best for nuclei that are well described by the Skyrme HF calculations. One such reaction is the fusion of ^{16}O+^{208}Pb system. In Fig. 2 we show an example of microscopic potentials for the ^{16}O+^{208}Pb system at three difference center-of-mass energies [6]. The dashed curves are the corresponding potentials transformed via the microscopically calculated effective mass, $M(R)$. We observe that all of the scaled barriers give a very good description of the fusion cross-section at higher energies suggesting these cross-sections

are primarily determined by the barrier properties in the vicinity of the barrier peak, whereas for the extreme sub-barrier cross-sections are influenced by what happens in the inner part of the barrier and here the dynamics and consequently the coordinate dependent mass becomes very important (see Fig. 3). Specifically, we can see from Fig. 2 that as the c.m. energy is increased the ion-ion potential peak increases but the inner part of the barrier becomes narrower. This is due to the fact that for high energies the system does not have enough time for rearrangements in the density to occur and the barrier approaches the frozen-density limit. However, at lower energies substantial density rearrangements occur which modifies the inner part of the barrier. This modification is important for fusion cross-sections are deep sub-barrier energies.

4.2. Deformed systems

The collision of the ^{64}Ni+^{132}Sn system represents a good example of a collision involving a deformed (oblate) nucleus, ^{64}Ni and a neutron rich nucleus. Fusion cross-sections for this system have been experimentally measured [20] and initially a significant discrepancy was observed with standard coupled-channel calculations. We have used the DC-TDHF method to study this system [3, 4]. The ion-ion potentials corresponding to two extreme orientations of the ^{64}Ni nucleus are shown in Fig. 4 as well as an empirical barrier used in barrier penetration calculations in Ref. [20]. Two important points are observed from this plot. The first is the strong dependence of the barrier height and location on the alignment of the deformed nucleus. We also see that the empirical barrier is very close to the equatorial orientation, which is closer to the assumption of spherical nuclei. The accuracy of our result with no parameters or normalization is impressive. The second point has to do with the meaning of *sub-barrier*; as seen from Fig. 4, while the experimental energies appear to be all sub-barrier with respect to the spherical barrier, two of them are above the barrier with respect to the $\beta = 90^o$ potential barrier and the third faces a considerably narrower barrier. This explains the anomalous observation of enhanced fusion at these energies.

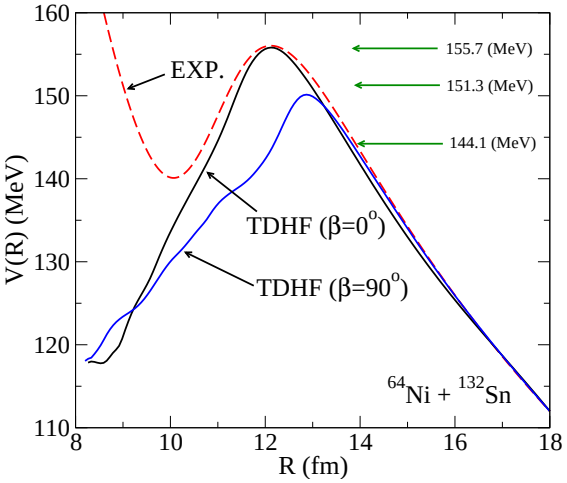

Figure 4. Potential barriers, $V(R, \beta)$, obtained from DC-TDHF calculations for the ^{64}Ni+^{132}Sn system. Angle β indicates different orientations of the deformed ^{64}Ni nucleus in $\Delta\beta = 10^\circ$ intervals. Also shown are the experimental energies.

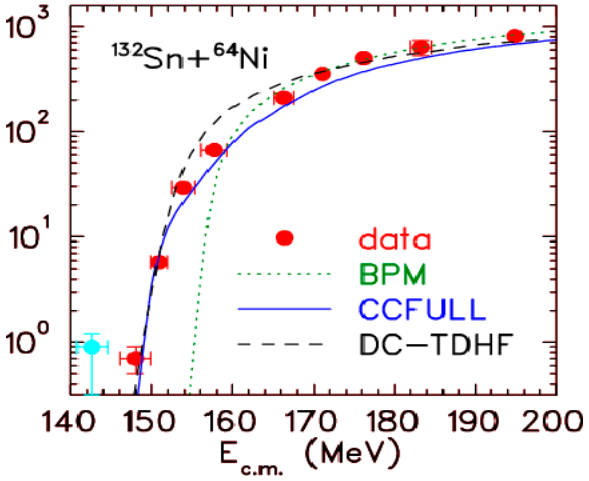

Figure 5. Total fusion cross section as a function of $E_{\rm c.m.}$. Shown are the experimental data (filled circles), the latest coupled-channel calculations [20] including neutron transfer (blue solid curve), and the DC-TDHF cross sections (dashed curve).

4.3. Superheavy systems

Ion-ion interaction potentials calculated using DC-TDHF correspond to the configuration attained during a particular TDHF collision. For light and medium mass systems as well as heavier systems for which fusion is the dominant reaction product, DC-TDHF gives the fusion barrier with an appreciable but relatively small energy dependence. On the other hand, for reactions leading to superheavy systems fusion is not the dominant channel at barrier top energies. Instead the system sticks in some dinuclear configuration with possible break-up after exchanging a few nucleons. For this reason the energy dependence of the DC-TDHF interaction barriers for these systems is not just due to the dynamical effects for the same final configuration but actually represent different final configurations. For the same reasons calculations presented here can only address the capture cross-section for these systems since the long-time evolution to complete fusion or break-up is beyond the scope of TDHF due to the absence of quantum decay processes and transitions.

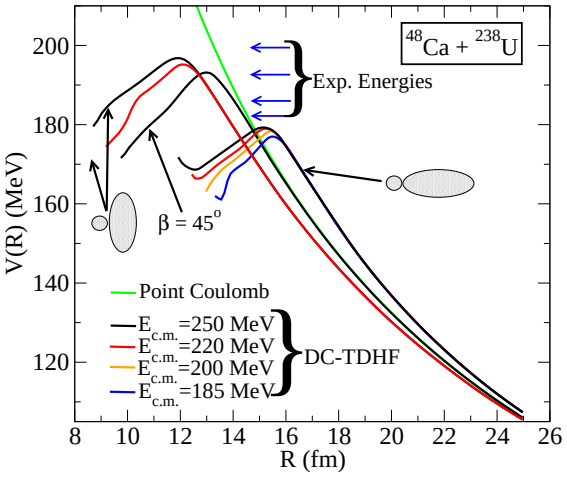

Figure 6. Potential barriers, $V(R)$, for the ^{48}Ca+^{238}U system obtained from DC-TDHF calculations as a function of $E_{\rm c.m.}$ energy and for selected orientation angles β of the ^{238}U nucleus. Also, shown are the experimental c.m. energies.

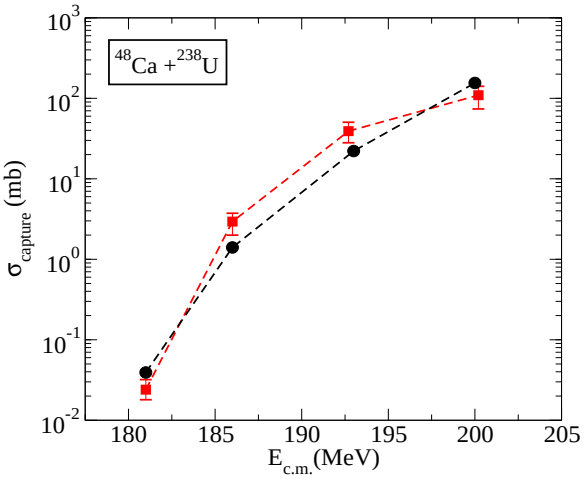

Figure 7. Capture cross-sections for the ^{48}Ca+^{238}U system as a function of $E_{\rm c.m.}$ energy (black circles). Also, shown are the experimental cross-sections (red squares) [21].

As an example of superheavy formation from a hot-fusion reaction we have studied the ^{48}Ca+^{238}U system [7]. Hartree-Fock (HF) calculations produce a spherical ^{48}Ca nucleus, whereas ^{238}U has a large axial deformation. The large deformation of ^{238}U is expected to strongly influence the interaction barriers for this system. This is shown in Fig. 6, which shows the interaction barriers, $V(R)$, calculated using the DC-TDHF method as a function of c.m. energy and for three different orientations of the ^{238}U nucleus. The alignment angle β is the angle between the symmetry axis of the ^{238}U nucleus and the collision axis. Also shown in Fig. 6 is the point Coulomb potential corresponding to this collision. The deviations from the point Coulomb potential at large R values are due to the deformation of the ^{238}U nucleus. We first notice that the barriers corresponding to the polar orientation ($\beta = 0^o$) of the ^{238}U nucleus are much lower and peak at larger ion-ion separation distance R. On the other hand, the barriers corresponding to the equatorial orientation of ^{238}U ($\beta = 90^o$) are much higher and peak at smaller R values. For the intermediate values of β the barriers rise rapidly as we increase the orientation angle from $\beta = 0^o$, as can be seen for $\beta = 45^o$. The rise in the barrier height as a function of increasing β values is not linear but seems to rise more rapidly for smaller β values.

We also see that for lower energies central collisions with polar orientation of ^{238}U are the only orientations which result in the sticking of the two nuclei, while the equatorial orientations of ^{238}U result in a deep-inelastic collision. Also, shown in Fig. 6 are the experimental energies [21] for this reaction. We observe that all of the experimental energies are above the barriers obtained for the polar alignment of the ^{238}U nucleus. For the calculation of the capture cross-section we need to average over all possible alignments of the ^{238}U nucleus. In Fig. 7 we show the capture cross-sections for the ^{48}Ca+^{238}U system as a function of $E_{\rm c.m.}$ energy (black circles). Also, shown are the experimental cross-sections (red squares) [21].

Acknowledgments
This work has been supported by the U.S. Department of Energy under grant No. DE-FG02-96ER40963 with Vanderbilt University.

References

[1] Umar A S and Oberacker V E 2006 *Phys. Rev.* C **74** 021601(R)
[2] Umar A S and Oberacker V E 2006 *Phys. Rev.* C **74** 024606
[3] Umar A S and Oberacker V E 2006 *Phys. Rev.* C **74** 061601(R)
[4] Umar A S and Oberacker V E 2007 *Phys. Rev.* C **76** 014614
[5] Umar A S and Oberacker V E 2008 *Phys. Rev.* C **77** 064605
[6] Umar A S and Oberacker V E 2009 *Eur. Phys. J.* A **39**, 243
[7] Umar A S, Oberacker V E, Maruhn J A and Reinhard P-G 2010 *Phys. Rev.* C **81** 064607
[8] Oberacker V E, Umar A S, Maruhn J A and Reinhard P-G 2010 *Phys. Rev.* C **82** 034603
[9] Negele J W 1982 *Rev. Mod. Phys.* **54** 913
[10] Cusson R Y, Reinhard P-G, Strayer M R, Maruhn J A and Greiner W 1985 *Z. Phys.* A **320** 475
[11] Umar A S, Strayer M R, Cusson R Y, Reinhard P-G and Bromley D A 1985 *Phys. Rev.* C **32** 172
[12] Chabanat E, Bonche P, Haensel P, Meyer J and Schaeffer R 1998 *Nucl. Phys.* A **635** 231; *Nucl. Phys.* A **643** 441
[13] Umar A S, Wu J , Strayer M R and Bottcher C 1991 *J. Comp. Phys* **93** 426
[14] Umar A S, Strayer M R, Reinhard P-G, Davies K T R and Lee S-J 1989 *Phys. Rev.* C **40** 706
[15] Davies K T R and Koonin S E 1981 *Phys. Rev.* C **23** 2042
[16] Boor C De 1978 *Practical Guide to Splines* (New York: Springer).
[17] Bottcher C, Strayer M R, Umar A S and Reinhard P-G 1989 *Phys. Rev.* A **40** 4182
[18] Umar A S and Oberacker V E 2006 *Phys. Rev.* C **73** 054607
[19] Umar A S, Strayer M R, Wu J-S, Dean D J and Güçlü M C 1991 *Phys. Rev.* C **44** 2512
[20] Liang J F *et al.* 2007 *Phys. Rev.* C **75** 054607
[21] Oganessian Yuri 2007 *J. Phys. G: Nucl. Part. Phys.* **34** R165